

See discussions, stats, and author profiles for this publication at: <https://www.researchgate.net/publication/385623669>

# Mapping indicator species of segetal flora for result-based payments in arable land using UAV imagery and deep learning

Article in Ecological Indicators · November 2024

DOI: [10.1016/j.ecolind.2024.112780](https://doi.org/10.1016/j.ecolind.2024.112780)

---

CITATIONS

0

READS

88

4 authors:



[Caterina Barraso](#)

German Centre for Integrative Biodiversity Research (iDiv) Halle-Jena-Leipzig

8 PUBLICATIONS 39 CITATIONS

[SEE PROFILE](#)



[Robert Krüger](#)

TU Dresden

14 PUBLICATIONS 28 CITATIONS

[SEE PROFILE](#)



[Anette Eltner](#)

TU Dresden

128 PUBLICATIONS 2,896 CITATIONS

[SEE PROFILE](#)

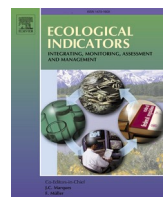
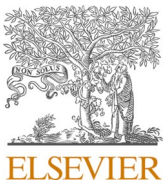


[Anna Cord](#)

University of Bonn

129 PUBLICATIONS 3,653 CITATIONS

[SEE PROFILE](#)



## Original Articles

## Mapping indicator species of segetal flora for result-based payments in arable land using UAV imagery and deep learning

Caterina Barrasso <sup>a,b,\*</sup>, Robert Krüger <sup>c</sup>, Anette Eltner <sup>c</sup>, Anna F. Cord <sup>a,b,d</sup><sup>a</sup> Chair of Computational Landscape Ecology, TUD Dresden University of Technology, Germany<sup>b</sup> Center for Scalable Data Analytics and Artificial Intelligence (ScADS.AI) Dresden/Leipzig, Germany<sup>c</sup> Institute of Photogrammetry and Remote Sensing, TUD Dresden University of Technology, Germany<sup>d</sup> Agro-Ecological Modeling Group, Institute of Crop Science and Resource Conservation, University of Bonn, Germany

## ARTICLE INFO

## ABSTRACT

## Keywords:

Segetal flora  
Indicator species  
Result-based payments  
Agricultural landscapes  
Deep learning  
UAV-based RGB imagery  
Ground sampling distance  
Point cloud

The decline of segetal flora species across Europe, driven by intensified agricultural practices, is impacting other taxa and ecosystem functions. Result-based payments to farmers offer an effective solution to conserve these species, but the high cost of biodiversity monitoring remains a challenge. In this study, we conducted UAV flights with an RGB camera and used the deep learning model YOLO to detect these species in four winter barley fields under different management intensities in Germany. Field measurements of plant traits were used to evaluate their impact on species detectability. Additionally, we investigated the potential of spatial co-occurrence and canopy height heterogeneity to predict the presence of species difficult to detect by UAVs. We found that half of the species observed could be remotely detected, with a minimum ground sampling distance (GSD) of 1.22 mm required for accurate annotation. The same detection ratio was estimated for key indicator species not present in our study area based on trait information. Plant height was crucial for species detection, with accuracy ranging between 49–100 %. YOLO models effectively predicted species from images taken at 40 m, reducing the monitoring time to eight minutes per hectare. Co-occurrence with UAV-detectable species and canopy height heterogeneity proved promising for identifying areas where undetectable species are likely to occur, although further research is needed for landscape-level applications. Our study highlights the potential for large-scale, cost-effective monitoring of segetal flora species in agricultural landscapes, and provides valuable insights for developing robust ‘smart indicators’ for future biodiversity monitoring.

## 1. Introduction

Segetal flora, naturally occurring vascular plants on agricultural land, are declining in Europe (Glaser et al., 2024) due to intensified farming practices (Carmona et al., 2020). While this concerns species in all farming systems (including tree crops; Piñar Fuentes et al., 2021), native species in winter cereal fields are among the most threatened (Fanfarillo et al., 2020a). The loss and homogenization of segetal flora communities has been associated with declines in other taxa, including arthropods (Bärberi et al., 2010) and vertebrates (Bowler et al., 2019), as well as with losses of essential ecosystem functions, such as nutrient retention and erosion reduction during fallow periods (Blaić et al., 2018). Effective management options to conserve segetal flora are known (Albrecht et al., 2016; Boetzel et al., 2021), but current action-based agri-environmental schemes designed around these practices

have failed to halt their decline in Europe (Pe'er et al., 2020).

A more effective alternative for biodiversity conservation are so-called result-based payments (RBPs) (Wuepper and Huber, 2022), that reward farmers for achieving specific biodiversity targets (e.g., plant species presence and/or abundance) on their land (Kaiser et al., 2019). Such RBPs, including species indicator lists on which payments are based, already exist for plant conservation in several European countries, but focus mainly on grasslands (Elmiger et al., 2023). Despite indications that farmers are willing to adopt such schemes (Massfeller et al., 2022), the implementation of RBPs for segetal flora on arable land has not yet been achieved, with the high cost for biodiversity monitoring remaining one of the major obstacles (Bartkowski et al., 2021).

Onsite plant surveys over extensive areas are time-consuming, costly, and can result in vegetation and crop damage. To tackle the issue, payments based on modeled results have been proposed (Bartkowski

\* Corresponding author.

E-mail address: [caterina.barrasso@tu-dresden.de](mailto:caterina.barrasso@tu-dresden.de) (C. Barrasso).

et al., 2021). However, advances in remote sensing have suggested that automated monitoring for RBPs using uncrewed aerial vehicles (UAVs) may become a viable technology (Schöttker et al., 2023), reducing not only costs and labor, but also enabling real-time monitoring. By operating at lower altitudes, UAVs are less constrained by weather conditions, and given the versatility of onboard sensors, have already been used to map different vegetation types. These include small herbaceous plant species in heterogeneous stands with high interspecies similarity in grasslands (Lu and He, 2017) and wetlands (Wolff et al., 2023).

Traditional machine learning approaches, such as random forest, require meticulous feature engineering to identify patterns (LeCun et al., 2015), which limits their ability to fully utilize the high spatial resolution of UAV-based imagery. Thus, it is more challenging to differentiate between numerous small herbaceous species with similar spectral signatures. For instance, using a simple UAV-based red-green-blue (RGB) camera, Lottes et al. (2017) were able to distinguish only two weed species (referred to as vegetal flora species in this study) in sugar beet arable fields using a random forest classifier. Similarly, Beyer et al. (2019) needed a more costly multispectral camera to distinguish eleven spectrally similar peatland species, along with an additional 3D model generated using Structure-from-Motion (SfM) to exploit plant height as an additional classification feature. By leveraging the optical feature space of UAV imagery, SfM offers a cost-effective approach to derive canopy height variability during vegetation assessments (Forsmoo et al., 2018, Torresani et al. 2024).

The advent of deep learning (DL) models, such as convolutional neural networks (CNNs), has enabled the automatic discovery of representations needed for detection and classification (LeCun et al., 2015). This has facilitated the exploitation of crucial traits of herbaceous plant species with overlapping spectral signatures (Liu et al., 2018). Even cheap RGB cameras (often already installed on commercial UAVs) can now distinguish a greater number of plant species (Kattenborn et al., 2020). By employing a UAV-based RGB camera and two DL models, Gallmann et al. (2022) and Martins et al. (2023) were able to successfully detect fourteen (flowering) and ten (non-flowering) herbaceous plant species in grasslands and kettle holes, respectively. However, a marginal decrease in predictive performance was observed up to a ground sampling distance (GSD) of 5 mm, while a significant decrease in accuracy was observed when GSD was further coarsened to 10 and 20 mm (Gallmann et al., 2022), suggesting that careful GSD selection based on the specific mapping objective is necessary.

Although previous studies have demonstrated the potential of UAV-based RGB cameras paired with DL models to detect herbaceous species, it remains largely unknown which species can be reliably detected based on their traits and what trade-offs in terms of GSD may exist for mapping vegetal flora in arable land. To address this knowledge gap, this study aimed to ascertain whether an off-the-shelf UAV-based RGB camera and a lightweight DL model, both of which are more readily affordable for a paying agency responsible for RBPs, can effectively detect vegetal flora species in arable land. We conducted UAV flights in June 2023 at different altitudes in an arable area of a UNESCO biosphere reserve in Germany, where winter barley was grown as the main crop under different management intensities. We aimed to map both dominant and sparsely growing plant species, and measured plant traits onsite to study their effect on detectability.

We hypothesized that plant traits such as plant height, flower diameter and species cover would play an important role in species-specific detectability. In addition, we hypothesized that i) GSD of UAV-based imagery would affect accuracy, but that a trained DL model would remain robust in generalizing across multiple flight heights, and ii) usage of canopy height heterogeneity (HH) derived from SfM and species co-occurrence analysis would assist in identifying areas within the field that are more likely to host UAV-undetectable species.

Specifically, we addressed the following research questions:

- i) Which vegetal flora species can be mapped with an off-the-shelf UAV-based RGB camera, and how do plant traits and GSD affect species-specific detectability and accuracy under different management intensities?
- ii) Do detectable and undetectable species spatially co-occur? Can canopy HH be used as a proxy to identify areas within the field where undetectable species are more likely to occur?

Finally, we aimed to extrapolate the potential of this workflow for mapping other species of vegetal flora not present in our study area by retrieving plant traits from the literature, thus supporting and facilitating a wider implementation of RBPs in Europe in the future.

## 2. Material and methods

### 2.1. Study area and workflow

The study area comprised four arable fields in the UNESCO Biosphere Reserve Upper Lusatian Heath and Pond Landscape, about 80 km northeast of Dresden, Germany ( $51.257^{\circ}$  N,  $14.572^{\circ}$  E; Fig. 1a). All fields were sown with winter barley (*Hordeum vulgare* L.), variety Lomerit NB, on loamy sand at an altitude of 188–202 m (GeoSN, dl-de/by-2-0, DGM1. Download: September 01, 2023). Two intensively managed fields (6.48 and 4.09 ha) received annual applications of fertilizers, dressing agents, fungicides, and herbicides. Two extensively managed fields (2.49 and 2.21 ha) were not subjected to such treatments, with the exception of the Rubin® TT seed dressing application.

Stratified random sampling was used to allocate 25 training/validation plots, with management type as stratum (Fig. 1a). Five plots were located in the intensively managed field, and 20 in the extensively managed field, where higher vegetal flora density was observed (Fig. 1b). In addition, 20 test plots were evenly split between management types to assess model accuracy. The *rSSI* function from the R package spatstat (Baddeley et al., 2005) was used to maintain a minimum 5 m distance during random allocation of the plots in each field. The workflow, implemented in R (v. 4.2.2) and Python (v. 3.10.4) is shown in Fig. 2. It involved: i) identifying UAV-detectable species, ii) training and assessing performance of a CNN segmentation model on RGB imagery, iii) testing spatial co-occurrence and canopy HH to predict UAV-undetectable species, iv) extrapolating the workflow to other species of interest for RBPs in arable land.

### 2.2. UAV-based data acquisition and processing

For data acquisition, we used the DJI M300 with a built-in receiver for positioning with real-time kinematic (RTK)-global navigation satellite system (GNSS) and an attached DJI Zenmuse P1 RGB camera (45MP full format sensor, 35 mm lens). UAV data was collected on 21 June 2023, during the flowering season and just before the onsite plant survey to avoid damaging the plots.

Flights were conducted under favorable weather conditions, with low wind speeds, between 10 am and 4 pm to avoid long shadows. Data collection included two types of flight missions: one over the designated plots and another over the entire extensive management area with test plots (Fig. 2). Plots were surveyed at altitudes of 10, 20, and 40 m with GSD and flight time detailed in Table 1. One test plot under intensive management was not overflowed due to its close proximity to trees. Additionally, each plot was photographed onsite with a Nikon camera (5 mm f/1.8 S lens) from 1.5 m height to facilitate RGB image labeling.

SfM photogrammetry in Agisoft Metashape (Version 2.0.1) was used to derive orthophotos and 3D models of the plots (PC<sub>P1</sub>) and the extensive field (PC<sub>40</sub>), with  $\sim 10^5$  points/m<sup>2</sup> and  $\sim 10^4$  points/m<sup>2</sup>, respectively. Each 3D model was georeferenced using only the RTK-GNSS positions of the images. More details on flight modes, image overlap and products' derivation are available in the UAV protocol (Appendix A).

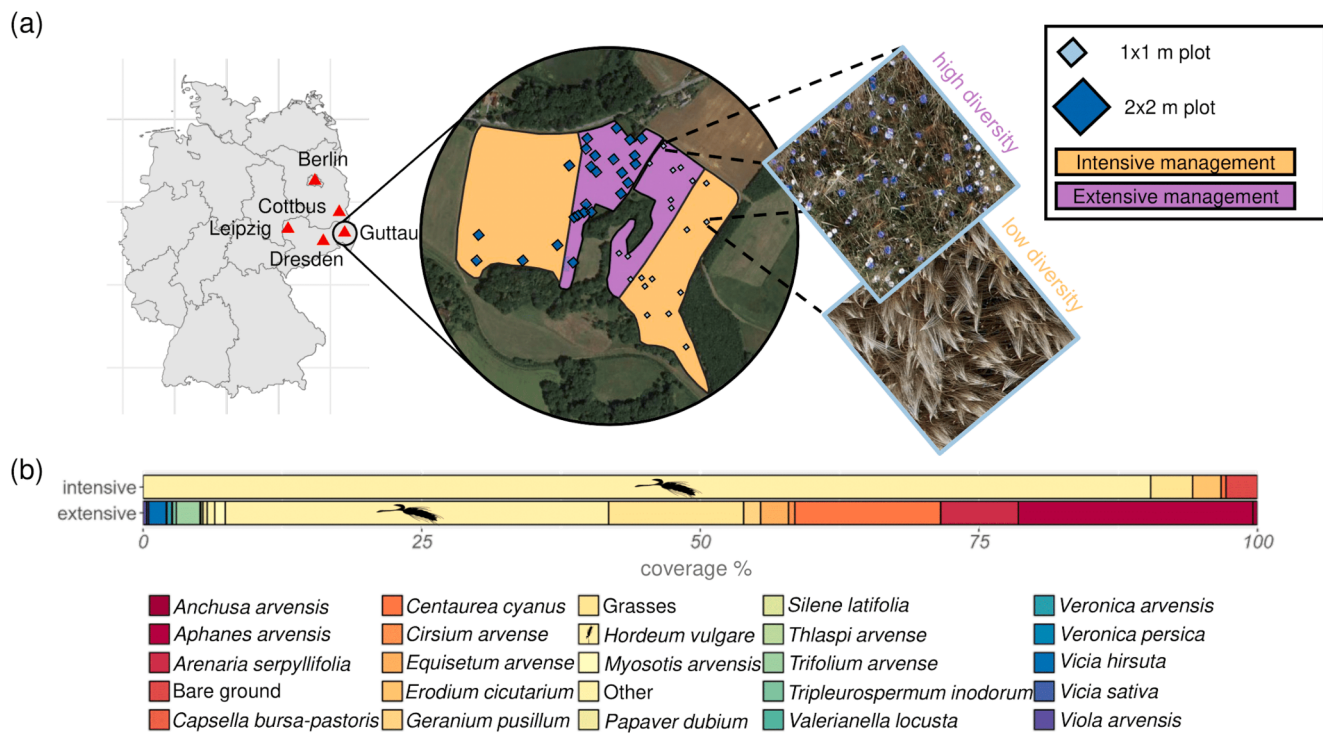


**Fig. 1.** (a) Study area consisting of four arable fields: two under intensive management (orange) and two under extensive management (pink). Diamonds indicate the distribution of training/validation plots (blue, 2x2 m) and test plots (sky blue, 1x1 m). Zoomed-in sky blue plots show examples of test plots per management type monitored using a UAV-based RGB camera at 10 m height. (b) Onsite vegetal flora species and winter barley coverage (%) in test plots across two management types where plant survey was conducted. Credits: Image of barley sourced from [www.vecteezy.com](http://www.vecteezy.com). (For interpretation of the references to color in this figure legend, the reader is referred to the web version of this article.)

### 2.3. Key indicator species

Since no accepted key indicators for plant-based RBPs on arable land exist (Elmiger et al., 2023), we developed a reference list of vegetal flora species. Following Keenleyside et al. (2014), indicator species were selected based on two principles important when designing RBPs: they must be i) easily identifiable, and ii) sensitive to changes in agricultural management, but otherwise stable. Vegetal flora species listed in Oppermann et al. (2021) and BfN (2024) were selected for their potential to enable time-efficient monitoring of European and German species in the field, respectively. Moss et al. (2004), Delbaere et al. (2009), and Ulber et al. (2009) guided the selection of species sensitive to changes in fertilization and/or herbicide application. If the easily identifiable species were not addressed by Moss et al. (2004), Delbaere et al. (2009), and Ulber et al. (2009), they were filtered based on their nitrogen requirements as outlined by Dengler et al. 2023. A value of seven or higher was considered indicative of nutrient-requiring species, while a value below this threshold indicated species preferring nutrient-poor soils. These latter species are generally considered key indicators of higher ecological value according to Fanfarillo and Kasperski (2021). Our final reference list consisted of 29 genera and 105 species (Table A1, Appendix A).

### 2.4. Plant survey

The onsite plant survey was conducted in test plots between June 22 and 24, 2023. We used a handheld RTK-GNSS receiver (Emlid Reach RS2+) to georeference the plots with ~1 cm accuracy. A species inventory was developed by identifying all species present in each test plot. Species identification was conducted using the FLORA incognita app, and their morphological characteristics were confirmed in the field using Jäger et al. (2017). Key indicator species cover was then estimated using a 9x9 grid of 5.5 cm equal squares, by counting the number of

equal squares where each species was present, divided by the total number and multiplied by 100. Additionally, we measured plant height, flower presence/absence, and flower diameter of three representative individuals per key indicator species per plot, if present.

### 2.5. Vegetal flora species detection and classification

To detect and classify vegetal flora species on UAV imagery, we trained the DL model “You Only Look Once” (YOLO) (Redmon et al., 2016) version 8, capable of instance segmentation (Jocher et al., 2023) and known for its favorable speed-accuracy trade-off (Terven et al., 2023). YOLOv8 is suitable for real-time detection with modest computational needs, and has been previously used for weed detection in wheat fields using smartphone images (Wang et al. 2024). The pre-trained medium version, *yolov8m-seg.pt*, was selected due to its average backbone network size, comprising 27.3 million parameters and a mean average precision (*mAP50 – 95<sup>mask</sup>*) of 40.8 (Jocher et al., 2023), offering a good balance between training efficiency and accuracy.

The Labelme software (Wada, 2016) was used for annotation, creating polygons in JSON format (Fig. A1, Appendix AA). Annotations were developed on RGB images captured at 10 m, where species recognition was more reliable. Seven species and one genus, among the observed key indicator species onsite, were visible on the UAV images, with their presence per plot additionally confirmed by the ground photographs taken with the Nikon camera. *Capsella-bursa pastoris* (L.) Medik. was rare, so only 14 annotations could be made. *Vicia sativa* L. and *Vicia hirsuta* (L.) Gray were undistinguishable, and thus aggregated at the genus level. YOLO models were thus trained and validated for the key indicator species listed in Table 2.

To improve processing of raw RGB images with the YOLO model, we created 36 non-overlapping tiles of 1,365 x 909 pixels, and added 10 % background images to reduce false positives (Jocher et al., 2023). The images were randomly split into five sets (80 % for training and 20 % for

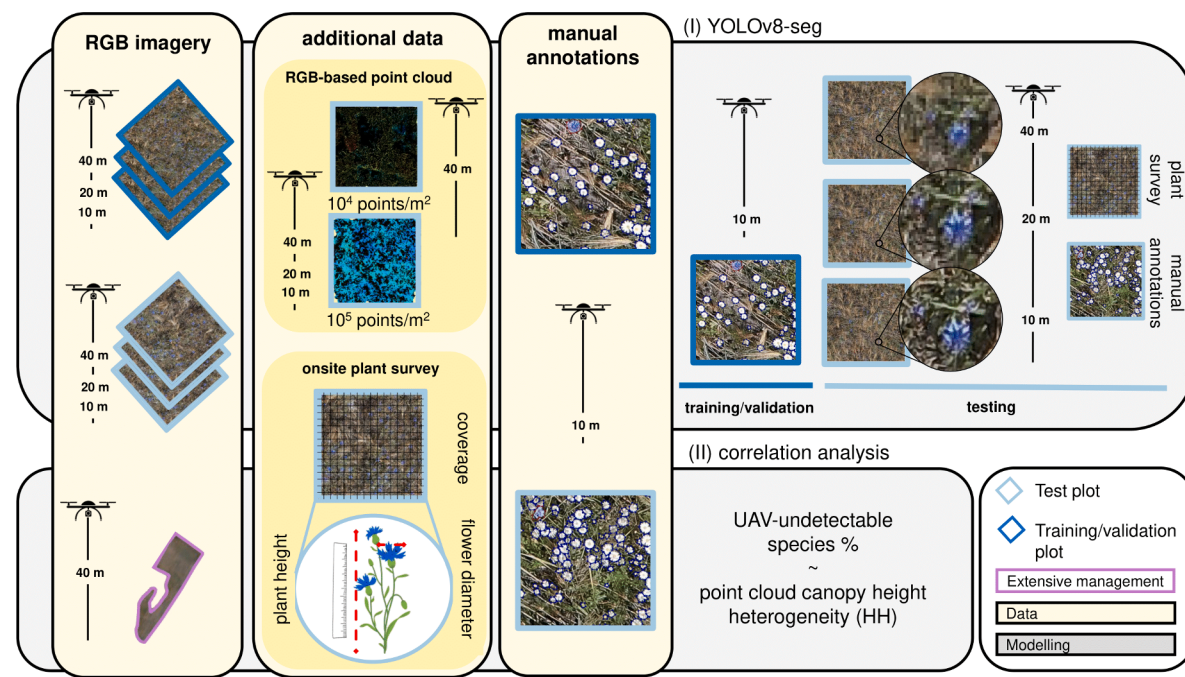


**Fig. 2.** Schematic overview of the study workflow (from left to right). UAV-based RGB images were captured at 10, 20, and 40 m over training/validation plots (blue) and test plots (sky blue) under both management types. High-resolution images at 10 m over training/validation plots were manually annotated to train the DL model (YOLOv8-seg) (I) for each species. Subsequently, the models were applied to images collected over test plots at three altitudes, and accuracy was evaluated against species cover and presence/absence data from manual annotation and plant survey. Plant height, species cover and flower diameter measured in the field were used to examine their effects on detectability. Under extensive management, the entire field containing test plots (see Fig. 1a) was monitored at 40 m. RGB-based point clouds were generated from i) images captured at the three altitudes over test plots (PC<sub>PI</sub> product), ii) images collected at 40 m over the entire extensive field, and later clipped to the test plots (PC<sub>40</sub> product). (II) A correlation analysis examined the relationship between canopy HH, derived from point cloud products, and UAV-undetectable species coverage. Credits: Image of cornflower and ruler sourced from [www.vecteezy.com](http://www.vecteezy.com). (For interpretation of the references to color in this figure legend, the reader is referred to the web version of this article.)

**Table 1**  
Altitude, GSD, and flight time per hectare for the conducted flights.

| Height (m) | GSD (mm) | Estimated flight time (mins/ha) |
|------------|----------|---------------------------------|
| 10         | 1.22     | 68                              |
| 20         | 2.44     | 35                              |
| 40         | 4.88     | 8.3                             |

validation) enabling five-fold cross-validation with default hyperparameters to establish baseline performance per species. The best performing data subset (Table 2) based on  $mAP_{50} - 95^{mask}$  was used for further hyperparameter tuning to find optimal species-specific hyperparameters and best model weights (Fig. A2-A8, Appendix A). Final segmentation loss, hyperparameters and mask F1 curve are shown in Fig. A9, Table A2, and Fig. A10 (Appendix A), respectively.

Plant height, flower diameter, and species cover per test plot were used as independent variables in a binomial regression, using the stats package (R Core Team, 2022), to analyze their effects on UAV species detection. Plant height and flower diameter were averaged over three individuals per species per plot, if present. Multi-model inference using the *dredge* function from the MuMin package (Bartoň, 2010) guided model selection, considering models within two  $\Delta AIC_c$  of the top model as competitive. The model with most variables was chosen to determine trait importance (Fig. A11a, Appendix A). The selected model was checked for assumptions and residuals using the DHARMA package (Hartig, 2016) (Fig. A11b, Appendix A), with significance reported at an alpha level of 0.05 (Fig. A11c, Appendix A).

## 2.6. Classification accuracy

The trained models were deployed on RGB orthomosaics developed

on test plots to evaluate model accuracy. Due to positional shifts and reconstruction variation observed between orthomosaics (Fig. A12, Appendix A), the 1.22 mm resolution orthomosaic (acquired at 10 m) was downsampled to 2.44 and 4.88 mm. We used the *aggregate* function, with mean calculation, from the raster package (Hijmans, 2010) to down-sample and investigate model transferability across GSDs. During inference, hyperparameters were kept at their optimized values during training, except for confidence threshold (set based on the optimal mask F1 curve value) and image size set to 864 (orthomosaic size at 10 m in test plots). Model run times across 19 plots at three heights with one GPU and 12 CPUs are shown in Table A4 in Appendix A.

Segmentation accuracy was assessed using the mean intersection over union (mIoU; Wang et al. 2023), precision and recall metrics calculated using manual annotations. Given potential omissions and discrepancies observed between species cover derived from manual annotations and survey data (Fig. A13, Appendix A), we additionally evaluated predicted coverage accuracy, using root mean square error (RMSE) and cosine similarity (Leydesdorff, 2005), and predicted presence/absence accuracy, using F1 score, with presence/absence data derived from species cover being larger or equal to zero. Kruskal-Wallis tests (Hollander and Wolfe, 1973) were used to check for significant differences between metrics, followed by Dunn's test with the rstatix package (Kassambara, 2019) for post-hoc multiple pairwise comparisons to study group differences.

## 2.7. Identification of areas within the fields with species undetectable by UAVs

Two methods were tested to identify areas within fields containing UAV-undetectable species. Firstly, we tested whether undetectable species spatially co-occurred with detectable species. Using presence-

**Table 2**

Number of annotations per species utilized to train and validate YOLO models following 5-fold cross-validation.

| Scientific Name  | Training (80 %) | Validation (20 %) |
|--|-----------------|-------------------|
|  <i>Anchusa arvensis</i> (L.) M.Bieb.             | 1,502           | 340               |
|  <i>Centaurea cyanus</i> L.                       | 4,692           | 1094              |
|  <i>Cirsium arvense</i> (L.) Scop.                | 1,348           | 299               |
|  <i>Equisetum arvense</i> L.                      | 1,507           | 423               |
|  <i>Papaver dubium</i> L.                        | 1,174           | 330               |
|  <i>Tripleurospermum inodorum</i> (L.) Sch.Bip. | 8,738           | 861               |
|  <i>Vicia</i> spec.                             | 1,270           | 330               |

\*Credits: Photos of species sourced from [Wikimedia Commons](#) CC0 1.0 Universal.

absence data from test plots, species co-occurrence was analyzed using the R package cooccur ([Griffith et al., 2016](#)), which categorizes pairs as having positive, negative, or random associations based on [Veech \(2013\)](#) probabilistic model. Pairs with an expected co-occurrence  $< 1$  were excluded from the analysis.

Secondly, we explored if canopy HH derived from two point-cloud products (PC<sub>PI</sub> and PC<sub>40</sub>) can serve as a proxy to identify areas within fields containing undetectable species. Thus, we conducted a correlation analysis between HH and the coverage of undetectable species, calculated by summing undetectable species coverage per test plot. We assumed that in small plots with similar soil and environmental conditions, crop plants would have uniform heights, thus variations in canopy HH can indicate the presence of other segetal flora species. Canopy HH per test plot was derived by calculating the standard deviation, the skewness and kurtosis (with the moments package; [Komsta and Novomestky, 2005](#)), and the Rao's Q (with the adiv package; [Pavoine, 2017](#)). The functions, implemented in the lidR package ([Roussel et al., 2020](#)), were used to derive canopy HH based on point cloud Z values and

empirical plant height measured in the field. Normality was assessed using the Shapiro-Wilk test from the stats package ([R Core Team, 2022](#)), with Pearson's correlation ([Pearson, 1895](#)) or Spearman's rank correlation ([Spearman, 1904](#)) applied based on data distribution. Correlations  $> 0.2$  and  $< 0.4$ ,  $\geq 0.4$  and  $< 0.6$ , and  $\geq 0.6$  and  $< 0.8$  were classified as weak, moderate and strong positive correlations, respectively. Post-hoc power analysis (0.8 power, 0.05 alpha, 0.6 correlation coefficient) was conducted to determine optimal sample size needed to detect significant correlations.

## 2.8. Assessment of transferability to other species based on traits

To estimate how remaining key indicator species, not present in our study area but relevant for RBPs ([Table A1, Appendix A](#)), could potentially be mapped with our workflow, we extracted mean plant height (referred to as mean from literature data) for each indicator from the GIFT ([Weigelt et al., 2020](#)) and BIEN ([Maitner, 2017](#)) datasets, using the R packages GIFT ([Denelle et al., 2023](#)) and BIEN ([Maitner et al., 2018](#)). To ensure comprehensive data retrieval, synonyms were checked on the [WFO Plant List](#). If plant height was unavailable, data for an indicator was marked as unknown to prevent inconsistencies from disparate data collection protocols.

We built a model to predict species detectability based on empirical plant height data. Each species in test plots was marked with value one if detectable, otherwise zero ([Table A5, Appendix A](#)). A binomial model was built with plant height as independent variable and detectability as response using the stats package ([R Core Team, 2022](#)) ([Fig. A14b, Appendix A](#)). Model assumptions and residuals were checked with the DHARMA package ([Hartig, 2016](#)) ([Fig. A14a, Appendix A](#)). Mean plant height from the two datasets was used to back-predict detectability of onsite species, determining a cut-off value of 0.21 based on the tallest undetectable species with a detection probability of 0.20. The binomial regression was then used to forecast detectability of the other key indicators. A species was deemed as “detectable” if its predicted probability exceeded 0.21, otherwise it was classified as “undetectable”.

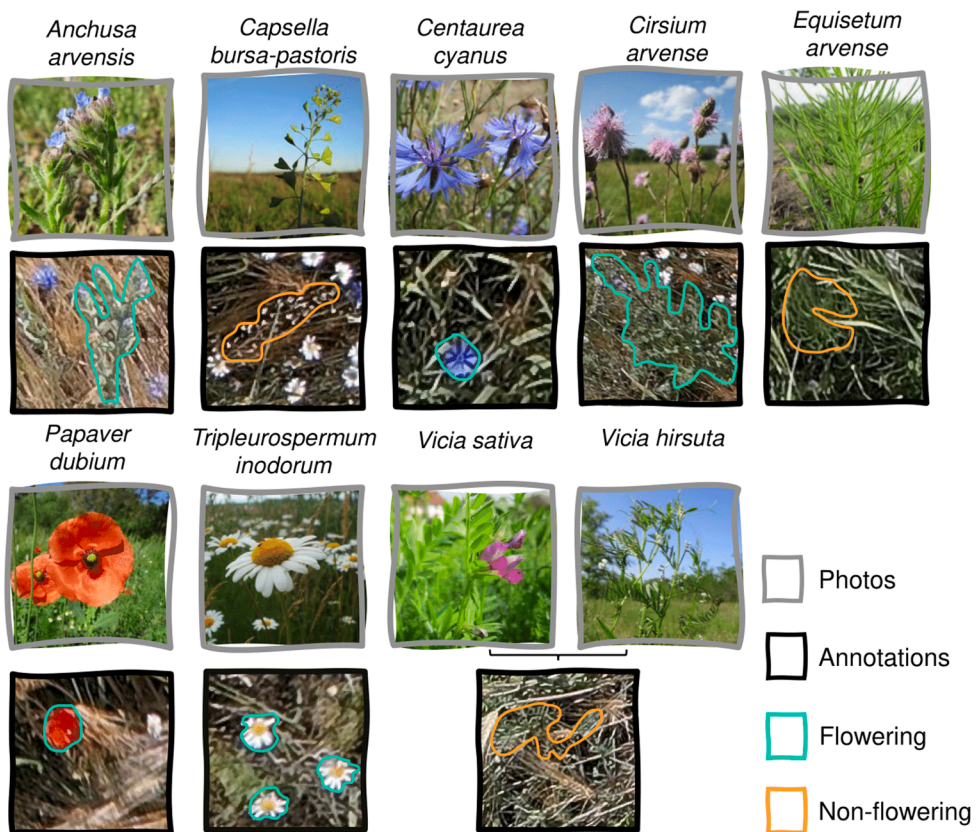
## 3. Results

### 3.1. Segetal flora species detection and classification accuracy

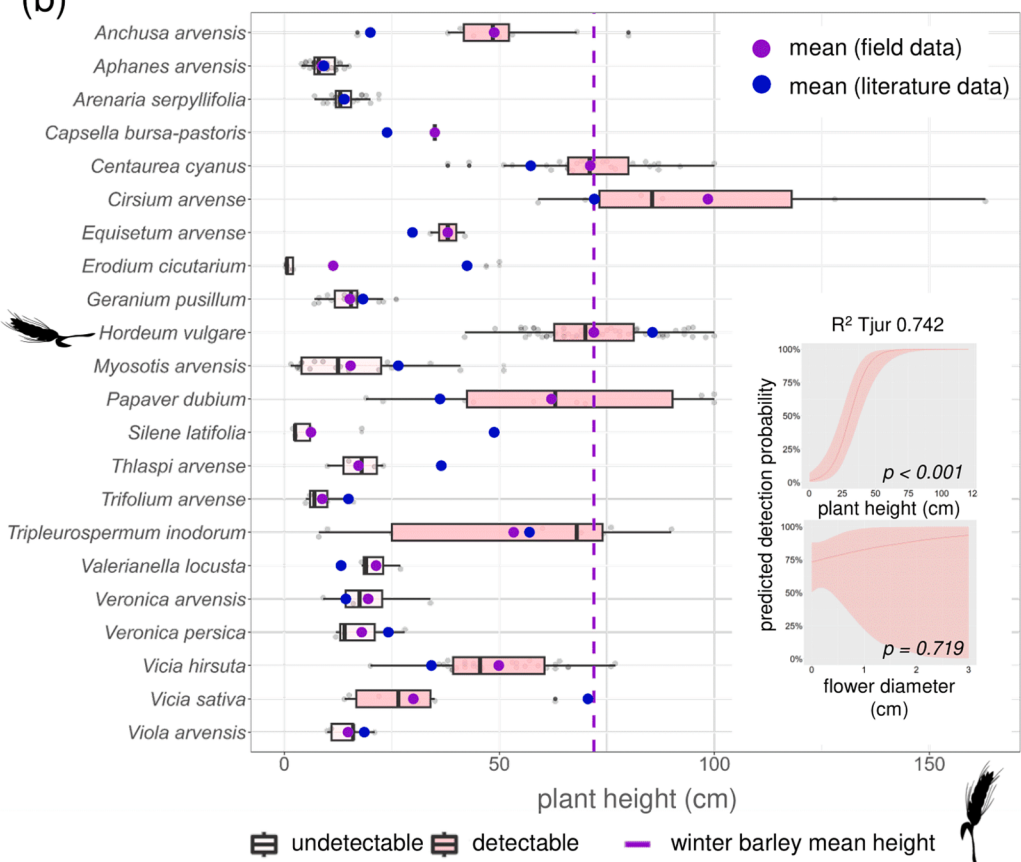
RGB images with 2.44 and 4.88 mm GSD were insufficient for confident species identification ([Fig. A12, Appendix A](#)), thus annotations were developed on high-resolution images of 1.22 mm GSD. Out of 21 key indicator species observed onsite ([Fig. 1b](#)), with greater abundance under low-input agriculture, nine species were detected on UAV imagery ([Fig. 3a](#)). *Anchusa arvensis*, *Capsella bursa-pastoris*, *Cirsium arvense* and *Vicia* species were annotated based on their full shoot system, while others were annotated based on floral structure alone. This can explain most of discrepancies observed between species cover derived with manual annotations and survey data ([Fig. A13, Appendix A](#)). Both flowering and non-flowering species were detected. Contrary to our expectations ([Table A5, Appendix A](#)), *Capsella bursa-pastoris* and *Vicia* species were not flowering during data collection. Non-flowering species and *Anchusa arvensis* were the most difficult to annotate due to lack of sharp boundaries (non-flowering species) and small flower size (*Anchusa arvensis*). Plant height was a more reliable indicator for species detection than flower diameter and species cover ([Fig. A11a, Appendix A](#)), with detection probability increasing with plant height ([Fig. 3b; R<sup>2</sup> = 0.742, p < 0.001](#)). The shortest detected species had a mean height 56 % shorter than the crop.

YOLO models for species with over 3,500 training instances were trained for more than 100 epochs, while those with fewer instances experienced early overfitting ([Fig. A9, Appendix A](#)). For all detected species, larger image size proved more beneficial than larger batch size, except for *Vicia* spec. ([Table A2, Appendix A](#)) which had the lowest mask F1 score (<0.1; [Fig. A10 in Appendix A](#)). *Anchusa arvensis* and *Equisetum*

(a)



(b)



(caption on next page)

**Fig. 3.** UAV-based detection of vegetal flora species. (a) Photos and examples of manual annotations for nine flowering and non-flowering species detected in our study, and categorized by flowering status (orange: non-flowering, cyan: flowering). (b) Bottom right: Effects of plant height and flower diameter on vegetal flora species detectability on UAV-based RGB images collected at 10 m above ground. Solid lines represent the model's marginal effects, with shaded bands indicating the 95 % confidence interval. On the left, the box plot compares the empirical plant height of detectable (pink) and undetectable (light pink) vegetal flora species and winter barley in the test plots. The mean plant height per species observed in the field (mean field data) is shown in purple, while the mean derived from the BIEN and GIFT datasets (mean literature data) is displayed in blue. Credits: Photos of species sourced from [Wikimedia Commons CC0 1.0 Universal](#). Vector of winter barley sourced from [www.vecteezy.com](#). (For interpretation of the references to color in this figure legend, the reader is referred to the web version of this article.)

*arvense* achieved higher mask F1 score than *Vicia* spec., but still below 0.5 during training. When segmentation accuracy was high, precision and recall were similar (Fig. 4a). Conversely, lower accuracy was associated with higher precision than recall. Trends in mIoU showed similar patterns, within species across management types and between species under same management type, at the three GSDs (Fig. 4b). *Vicia* spec. showed significantly lower mIoU under extensive management compared to intensive agriculture, with a mean mIoU of 0.49 versus 0.72 to 0.87 for other species. Under intensive management, mean mIoU improved to 0.74 (*Anchusa arvensis*), 0.99 (*Centaurea cyanus*), 1 (*Cirsium arvense*), 0.94 (*Equisetum arvense*), 1 (*Papaver dubium*), 1 (*Tripleurospermum inodorum*), and 0.98 (*Vicia* spec.).

Species cover estimates from manual annotations were consistently lower than those from onsite survey, except for *Cirsium arvense* and *Vicia* spec. (Fig. A13, Appendix A). However, coverage (cosine similarity) and presence/absence (F1) accuracies showed no significant differences within GSD across management types or between GSDs under same management type (Fig. 5). Under extensive management, cosine similarity was lower with survey data, but still ranged between 0.62 and 0.64. Significant differences in coverage accuracy (RMSE) were observed between management types at 2.44 mm and 4.88 mm GSDs (with manual annotations) and at 4.88 mm GSD (with field survey data), with lower RMSE observed under intensive management.

### 3.2. Identification of field areas with UAV-undetectable species

Out of 231 possible species pairs, 133 pairs (57.58 %) with expected co-occurrence  $< 1$  were excluded from the co-occurrence analysis (see section 2.7). Among the analyzed pairs, 29 showed positive co-occurrence, while none showed negative co-occurrence (Fig. 6a). Detected species such as *Vicia hirsuta*, *Centaurea cyanus*, *Anchusa arvensis*, *Papaver dubium* and *Tripleurospermum inodorum* showed positive co-occurrence with some undetected species.

Strong ( $R = 0.63, p = 0.0038$ ;  $R = 0.78, p < 0.05$ ) to moderate ( $R = 0.49, p = 0.032$ ) positive correlations were found between HH, from PC<sub>pl</sub> product and onsite plant height, and the percentage of UAV-undetectable species under both management types (Fig. 6b). In contrast, weak positive and non-significant correlations were observed between the percentage of UAV-undetectable species and HH measured with PC<sub>40</sub> product and onsite plant height under extensive management alone. Onsite plant height, based on three individuals per species per plot (see section 2.4), provides fewer data points than point cloud products to derive HH. Discrepancy was observed between Z-value densities of the two products, with the PC<sub>pl</sub> product showing higher densities at shorter heights (Fig. 6c). Post-hoc power analysis indicated that, under the extensive management alone, sample size was insufficient to reject the null hypothesis of zero correlation (Fig. A15, Appendix A).

### 3.3. Potential for RBPs targeting other species based on traits

Of the selected indicator species, 72 (54 %) are potentially detectable with a UAV-based RGB camera based on literature mean plant height and our detection model developed on empirical data (Fig. 7). Information could not be predicted for 13 % of the species. In the field, approximately 50 % of the observed species had mean plant heights differing by 30 % from those in the GIFT and BIEN datasets (Fig. 3b). Winter barley was found to be 21.1 and 5.1 cm shorter than the

literature estimate under extensive and intensive management, respectively.

## 4. Discussion

This study assesses the effectiveness of an off-the-shelf UAV-based RGB camera and the YOLO model for detecting vegetal flora species under different management intensities in arable land with winter barley grown as main crop. Building on previous research by Schöttker et al. (2023), which demonstrated the potential of UAVs for RBPs targeting floral cover in grassland, we focus on species detectability and GSD trade-offs using a cost-effective monitoring system. Furthermore, we investigated the potential use of canopy HH and species co-occurrence to identify areas where UAV-undetectable species may occur.

The developed list of key indicator species can serve as a basis for monitoring European vegetal flora, though further consensus is needed to consider and prioritize their beneficial ecological functions (Gazoulis et al., 2024) for future locally adapted RBPs. Our results align with earlier studies (Storkey et al., 2012; Carmona et al., 2020) that found vegetal flora to be more abundant under extensive management. One of the species in our study, *Cirsium arvense*, has been previously detected by UAVs in kettle holes (Martins et al., 2023). Although previous studies have used UAVs to distinguish between flowering species of the same genus (Gallmann et al., 2022), our findings indicate that *Vicia sativa* and *Vicia hirsuta* were undistinguishable. However, they were not in flower during our data collection, even though they were expected to be.

Approximately half of the onsite species were detected using UAV imagery, requiring a minimum GSD of 1.22 mm to develop accurate annotations. This aligns with Gallmann et al. (2022), who used a similar GSD for UAV-based annotations of flowering plant species in grasslands. Contrary to our expectations, species detection was more influenced by plant height than by flower diameter or species coverage. The shortest detected species had a mean height 56 % shorter than winter barley. The results suggested that plant height is the critical factor for effective detection at a given GSD in crop stands, with species around half the height of winter barley remaining discernible. These findings mirror challenges in detecting understory species in forest ecosystems using remote sensing, where overstory canopy often obstructs visibility (Yang et al., 2023).

Our study demonstrates that an off-the-shelf UAV-based RGB camera coupled with YOLO architecture can achieve vegetal flora segmentation accuracy between 49 and 100 %, depending on species and management type, with an average deployment speed  $< 0.5 \text{ sm}^{-2}$ . The detectability model, based on empirical data, indicated that this approach can detect 50 % of the indicator species in our list. Notwithstanding discrepancies between empirical and literature-derived mean plant heights, particularly under extensive management, the ratio of detectable to undetectable species remained consistent with our field data. YOLO's speed-accuracy trade-off worked well for most species, but accuracy for *Anchusa arvensis* and *Vicia* spec. was  $< 80$  %. The lower accuracy likely stems from the suboptimal number of annotations used during training for these challenging-to-annotate species (Basavegowda, 2024). Exploring other lightweight architectures, such as DeepLabV3 (Chen et al., 2018) known for its high accuracy in fine-scale segmentations, may improve results for these species.

Our models, trained on high-resolution images, can be effectively applied to RGB images with a GSD of 4.88 mm without significant

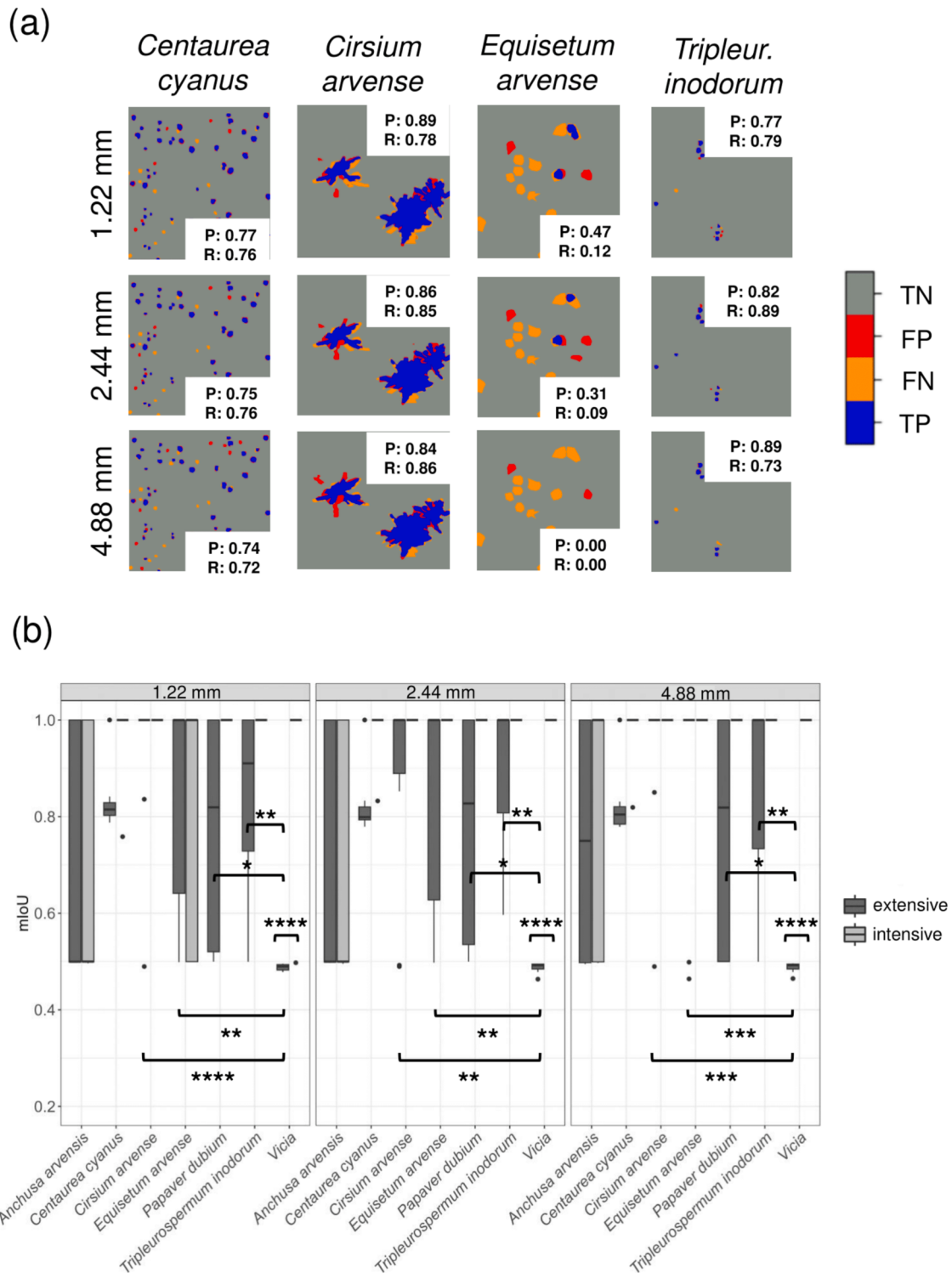


**Fig. 4.** (a) Examples of YOLO inferences for four species in test plots across three GSDs (1.22, 2.44 and 4.88 mm). *Centaurea cyanus* and *Equisetum arvense* are predicted in plot 26, while *Cirsium arvense* and *Tripleurospermum inodorum* are predicted in plots 32 and 33, respectively. Colors indicate: blue (true positives, TP), orange (false negatives, FN), red (false positives, FP), grey (true negatives, TN). Precision and recall for each plot are denoted by P and R. (b) mIoU accuracy per species and management type at three GSDs tested. Dunn's post-hoc results are shown with significance levels: \* =  $p < 0.05$ , \*\* =  $p < 0.01$ , \*\*\* =  $p < 0.001$ , \*\*\*\* =  $p < 0.0001$ . Only significant differences within species across management types or between species under same management type are reported. (For interpretation of the references to color in this figure legend, the reader is referred to the web version of this article.)

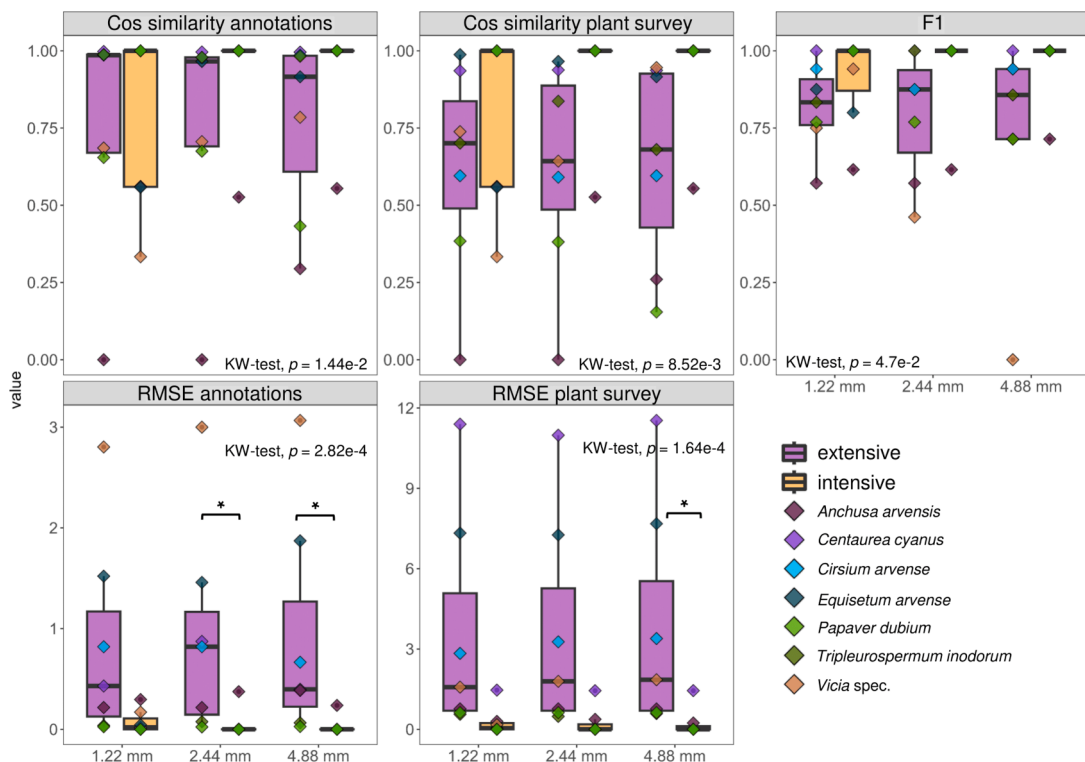


**Fig. 5.** Differences in coverage accuracy (cosine similarity and RMSE) and presence/absence accuracy (F1) across management types and GSDs, aggregated across the seven detectable species in test plots. Coverage accuracy is evaluated using both manual annotations and field survey data. Dunn's post-hoc results are shown with significance levels: \* =  $p < 0.05$ , \*\* =  $p < 0.01$ , \*\*\* =  $p < 0.001$ , \*\*\*\* =  $p < 0.0001$ . Only significant differences within GSD across management types or between GSDs under same management type are reported.

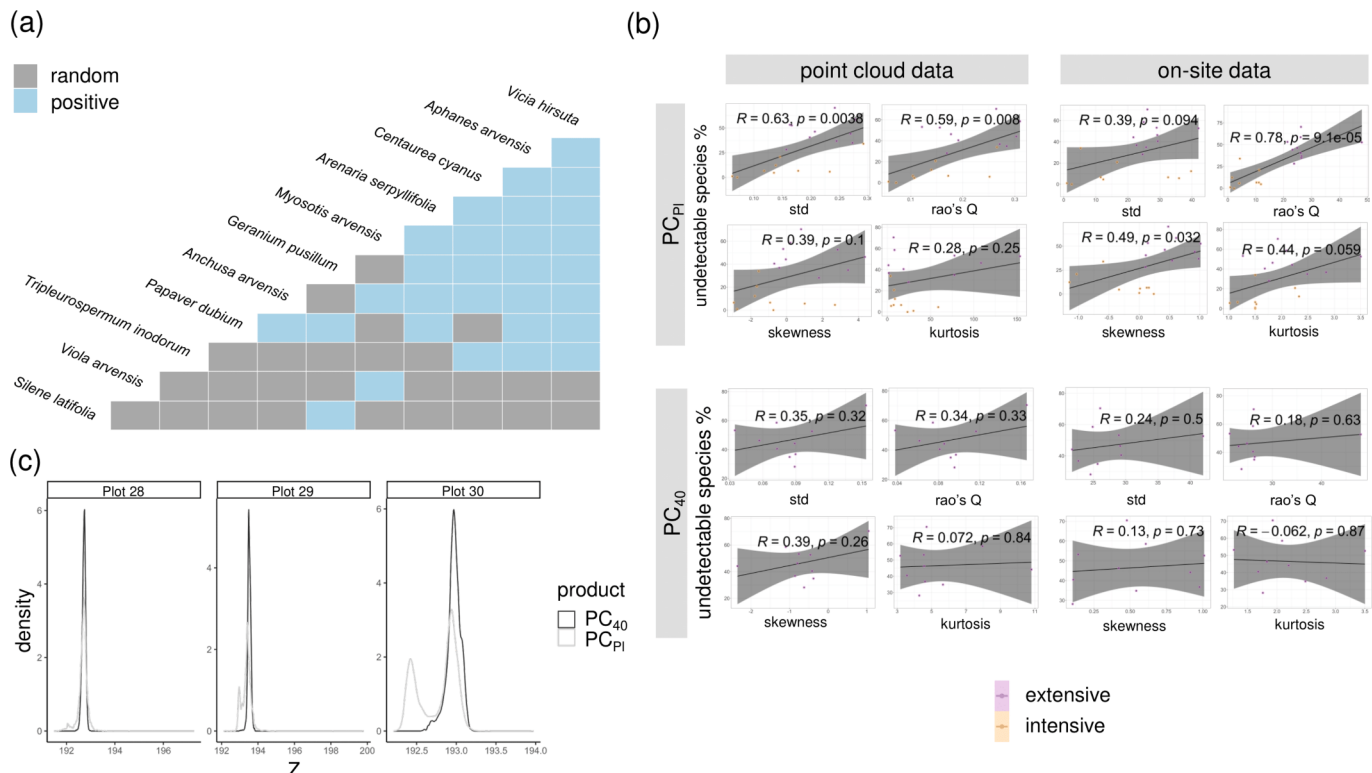


**Fig. 6.** (a) Co-occurrence of vegetal flora species and winter barley in test plots under two management types. Sky blue indicates positive co-occurrence, and grey indicates random co-occurrence. (b) Correlation analysis between canopy HH, derived from point cloud products (PC<sub>PI</sub> and PC<sub>40</sub>) and onsite plant height data, and UAV-undetectable species percentage in test plots. HH is expressed by standard deviation (std), Rao's Q, skewness and kurtosis. Analysis includes PC<sub>PI</sub> product under both management intensities and PC<sub>40</sub> product under extensive management where the point cloud was produced (see section 2.2). Solid lines represent regression lines, and shaded bands show the 95% confidence interval. (c) Density difference of point cloud Z-values in three test plots (plots 28–30) per product type (PC<sub>PI</sub> in grey, PC<sub>40</sub> in black). (For interpretation of the references to color in this figure legend, the reader is referred to the web version of this article.)

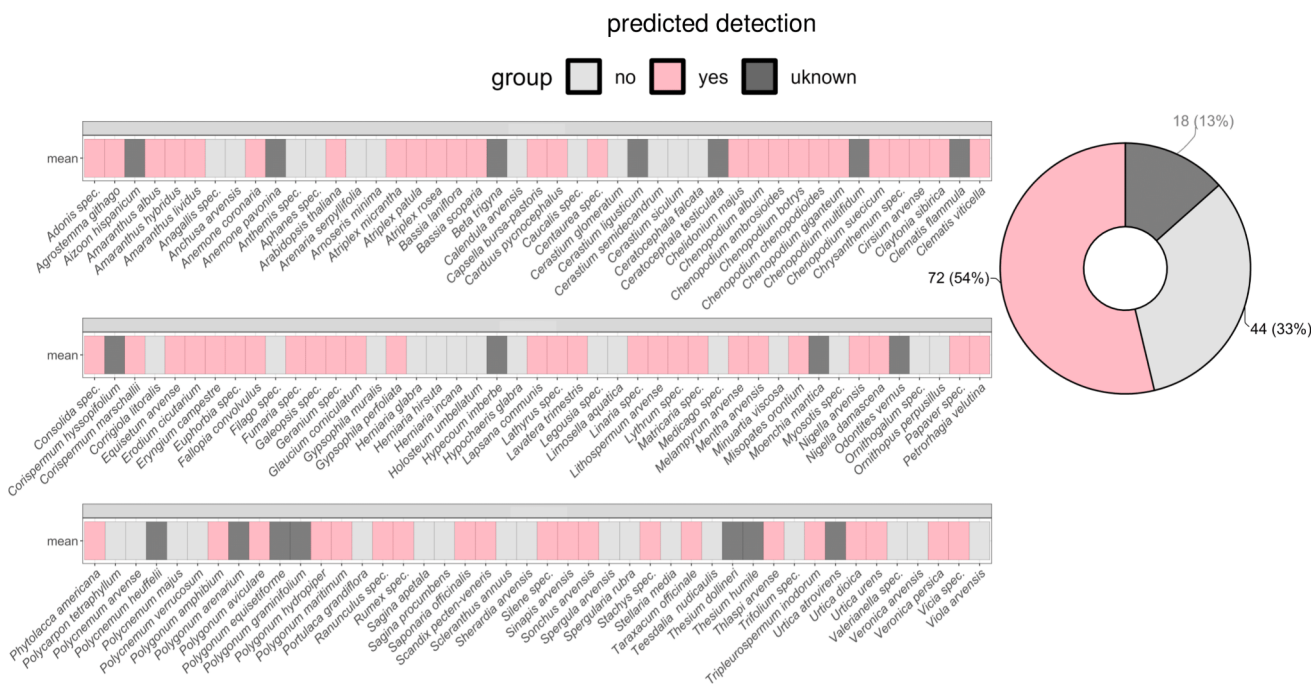


**Fig. 7.** Predicted detectability of each key indicator species selected in the study (aggregated value in pie graph) based on mean plant height retrieved from the literature. Categories are color-coded as follows: pink (detectable), dove grey (undetectable), and dark grey (unknown). (For interpretation of the references to color in this figure legend, the reader is referred to the web version of this article.)

accuracy loss, making it feasible for rapid monitoring of large areas. Similar CNN performance in mapping flowering plant species in grasslands with UAV-based imagery up to 5 mm GSD was reported by Gallmann et al. (2022). However, while YOLO can most likely generalize well across scales due to its standard augmentation runs designed to improve accuracy (Redmon et al., 2016), higher accuracy in predicting species cover was observed under intensive management at coarser GSDs of 2.44 and 4.44 mm. Future research should involve training models with species annotations developed at multiple scales to reduce differences in coverage accuracy observed between management types at coarser GSDs.

Our study suggests that co-occurrence with UAV-detectable species and canopy HH from a 3D point cloud derived by SfM can potentially constrain field areas where undetectable species are more likely to occur. For instance, *Centaurea cyanus* co-occurred with four undetectable species in our study. Fanfarillo et al. (2020b) found *Centaurea cyanus* to co-occur with *Veronica arvensis* and *Viola arvensis*, both undetectable but not co-occurring with *Centaurea cyanus* in our study. Developing species co-occurrence matrices under different environmental gradients and for different species pools may assist European countries in defining expected understory species associated with detectable ones. This may be greatly facilitated by considering phytosociological alliances recently being developed at the European level by Preislerová et al. 2022, in conjunction with the relevant edaphic factors underpinning plant growth. HH from the PC<sub>PI</sub> product effectively identified field areas with a higher probability of undetectable species, unlike the PC<sub>40</sub> product. PC<sub>PI</sub> showed higher density at shorter heights, suggesting it can capture more detail beneath the canopy. Developing a PC<sub>PI</sub> product, though, is impractical for entire fields due to long flight times at low altitudes. Additionally, our post-hoc power analysis indicated insufficient sample size to confirm significant correlation with the PC<sub>40</sub> product. Thus, further research is needed to assess whether SfM-derived point cloud at 40 m can effectively identify areas with undetectable species. The restricted field areas can then be monitored onsite for species identification. Alternatively, adaptive planning algorithms could dynamically adjust UAV flight altitudes to focus on specific areas (Stache et al., 2023), given that higher image resolution has been shown

to improve understory species mapping (Hernandez-Santin et al., 2019).

Future work will require additional UAV-based imagery at around 1 mm GSD to train YOLO models for other indicator species. Achieving this GSD may involve different altitudes or camera specifications, such as focal length and pixel pitch (Eltner and James, 2022). Since plant phenology impacts model performance (Gallmann et al., 2022), generating annotations for different flowering stages could enhance accuracy in fields with slight phenological shifts. However, distinguishing non-flowering species within the same genus may remain a significant challenge that may only be overcome through the use of more advanced sensors, such as hyperspectral sensors (Mensah et al. 2024). While we expect our models to generalize across winter cereals fields, further testing in different areas with different crops (e.g. summer cereals or tree crops) is needed to identify effective “smart indicators” and validate UAV-detectability for indicator species as postulated in this study.

## 5. Conclusions

This study demonstrates that vegetal flora species can be effectively monitored using an off-the-shelf UAV-based RGB camera and the YOLO DL model, enabling large-scale, cost-effective monitoring for broader implementation of RBPs in European agricultural landscapes. Plant height is a critical factor for species detectability, with about half of the key indicator species that can be detectable with this approach and can serve as “smart indicators” by farmers and paying agencies. The developed models can predict species cover on RGB images captured at 40 m, allowing to monitor one hectare of land in about eight minutes. Co-occurrence between species and canopy HH derived with SfM show promise to identify field areas where understory species may occur, though further research is needed to make these tools applicable at landscape level. Future studies should: i) validate UAV-based detectability of key indicators defined in this study, ii) assess models’ performance in other winter barley fields, and iii) refine species annotations in diverse regions with different main crops grown.

## CRediT authorship contribution statement

**Caterina Barrasco:** Writing – original draft, Visualization, Methodology, Investigation, Formal analysis, Conceptualization. **Robert Krüger:** Writing – review & editing, Methodology, Investigation, Conceptualization. **Anette Eltner:** Writing – review & editing, Methodology, Conceptualization. **Anna F. Cord:** Writing – review & editing, Supervision, Methodology, Conceptualization.

## Declaration of competing interest

The authors declare that they have no known competing financial interests or personal relationships that could have appeared to influence the work reported in this paper.

## Acknowledgments

CB received financial support from the German Federal Ministry of Education and Research (BMBF) and the Saxon State Ministry of Science, Culture and Tourism (SMWK) by funding the “Center for Scalable Data Analytics and Artificial Intelligence Dresden/Leipzig”, project identification number: SCADS24B. RK was funded by the Horizon Europe project EarthBridge (grant agreement no. 101079310). AFC was supported by the Deutsche Forschungsgemeinschaft (DFG, German Research Foundation) under Germany’s Excellence Strategy – EXC 2070 – 390732324. Views and opinions expressed are, however, those of the authors only and do not necessarily reflect those of the European Union. Neither the European Union nor the granting authority can be held responsible for them. The authors gratefully acknowledge the GWK support for funding this project by providing computing time through the Center for Information Services and HPC (ZIH) at TU Dresden. We would like to thank the UNESCO biosphere reserve “Upper Lusatian Health and Pond Landscape” and the agricultural cooperative “Heidefarm Sdier eG” for allowing us to collect the data for this study and for logistic support. We further thank others who helped with data collection and labeling of the images, in particular Sophia Lewitz, Bela Rehnen, Stephanie Roilo and Anja Steingrobe.

## Appendix A. Supplementary data

Supplementary data to this article can be found online at <https://doi.org/10.1016/j.ecolind.2024.112780>.

## Data availability

Data and models to reproduce the findings of our study are accessible in Appendix A and archived in Zenodo at: <https://doi.org/10.5281/zenodo.13983340> (Barrasco, 2024). Requests for manual annotations used for training and validation of the YOLO models can be submitted to the corresponding author. The R and Python code produced for the aforementioned analyses are available for download at <https://github.com/barrakat/SegFlora>.

## References

- Albrecht, H., et al., 2016. Management options for the conservation of rare arable plants in Europe. *Bot. Lett.* 163 (4), 389–415. <https://doi.org/10.1080/2381807.2016.1237886>.
- Baddeley, A., Turner, R., 2005. spatstat: an R package for analyzing spatial point patterns. *J. Stat. Softw.* 12 (6). <https://doi.org/10.18637/jss.v012.i06>.
- Bàrberi, P., et al., 2010. Functional biodiversity in the agricultural landscape: relationships between weeds and arthropod fauna. *Weed Res.* 50 (5), 388–401. <https://doi.org/10.1111/j.1365-3180.2010.00798.x>.
- Barrasco, C., 2024. UAV SegetalFlora. Zenodo. <https://doi.org/10.5281/zenodo.13983340>.
- Bartkowski, B., et al., 2021. Payments by modelled results: a novel design for agri-environmental schemes. *Land Use Policy* 102, 105230. <https://doi.org/10.1016/j.landusepol.2020.105230>.
- Bartoní, K., 2010 ‘MuMIn: Multi-Model Inference’. <https://doi.org/10.32614/CRAN.package.MuMin>.
- Basavegowda, D.H., 2024. ‘Deep Learning-based UAV-assisted grassland monitoring to facilitate Eco-scheme 5 realization’. <https://dl.gi.de/server/api/core/bitstreams/49be3f8-c4ca-41b4-af3c-38f111988d54/content>.
- Beyer, F., et al., 2019. Multisensor data to derive peatland vegetation communities using a fixed-wing unmanned aerial vehicle. *Int. J. Remote Sens.* 40 (24), 9103–9125. <https://doi.org/10.1080/01431161.2019.1580825>.
- BfN, 2024. ‘Erfassungsanleitung für den HNV-Farmland-Indikator’, Version 14. [https://www.bfn.de/sites/default/files/2024-04/Erfassungsanleitung\\_HNV\\_V14\\_2024.pdf](https://www.bfn.de/sites/default/files/2024-04/Erfassungsanleitung_HNV_V14_2024.pdf).
- Blaix, C., et al., 2018 ‘Quantification of regulating ecosystem services provided by weeds in annual cropping systems using a systematic map approach’, *Weed Research*. Edited by L. Rew, 58(3), pp. 151–164. <https://doi.org/10.1111/wre.12303>.
- Boetzel, F.A., et al., 2021. A multitaxa assessment of the effectiveness of agri-environmental schemes for biodiversity management. *Proc. Natl. Acad. Sci.* 118 (10), e2016038118. <https://doi.org/10.1073/pnas.2016038118>.
- Bowler, D.E., et al., 2019. Long-term declines of European insectivorous bird populations and potential causes. *Conserv. Biol.* 33 (5), 1120–1130. <https://doi.org/10.1111/cobi.13307>.
- Carmona, C.P., et al. 2020. Agriculture intensification reduces plant taxonomic and functional diversity across European arable systems, *Functional Ecology*. Edited by C. Seymour, 34(7), pp. 1448–1460. <https://doi.org/10.1111/1365-2435.13608>.
- Chen, L.C., et al. 2018. ncoder-Decoder with Atrous Separable Convolution for Semantic Image Segmentation, in V. Ferrari et al. (eds) *Computer Vision – ECCV 2018*. Cham: Springer International Publishing (Lecture Notes in Computer Science), pp. 833–851. [https://doi.org/10.1007/978-3-030-01234-2\\_49](https://doi.org/10.1007/978-3-030-01234-2_49).
- Delbaere, B., et al., 2009. BioScore: A tool to assess the impacts of European Community policies on Europe’s biodiversity. <https://www.synbiosys.alterra.nl/bioscore/download/BioScore%20final%20report.pdf>.
- Denelle, P., Weigelt, P., Kreft, H., 2023. GIFT — an R package to access the global inventory of floras and traits. *Methods Ecol. Evol.* 14 (11), 2738–2748. <https://doi.org/10.1111/2041-210X.14213>.
- Dengler, J., et al., 2023. Ecological indicator values for Europe (EIVE) 1.0. *Veg. Classif. Surv.* 4, 7–29. <https://doi.org/10.3897/VCS.98324>.
- Eltner, A., James, M., 2022 ‘Guidelines for flight operations’, pp. 76–84. In: Eltner, A., et al., 2022. UAVs for the Environmental Sciences – Methods and Applications. Teaching book, WBG Academic. <https://tud.link/18na18>.
- Elmiger, B.N., et al., 2023. Biodiversity indicators for result-based agri-environmental schemes – current state and future prospects. *Agr. Syst.* 204, 103538. <https://doi.org/10.1016/j.agry.2022.103538>.
- Fanfarillo, E., et al., 2020a. The segetal flora of winter cereals and allied crops in Italy: species inventory with chorological, structural and ecological features. *Plant Biosystems - An International Journal Dealing with All Aspects of Plant Biology* 154 (6), 935–946. <https://doi.org/10.1080/11263504.2020.1739164>.
- Fanfarillo, E., Kasperski, A., 2021. An index of ecological value for European arable plant communities. *Biodivers. Conserv.* 30 (7), 2145–2164. <https://doi.org/10.1007/s10531-021-02191-x>.
- Fanfarillo, E., Latini, M., Abbate, G., 2020b. Patterns of co-occurrence of rare and threatened species in winter arable plant communities of Italy. *Diversity* 12 (5), 195. <https://doi.org/10.3390/d12050195>.
- Forsmoo, J., et al., 2018. Drone-based structure-from-motion photogrammetry captures grassland sward height variability. *J. Appl. Ecol.* 55. <https://doi.org/10.1111/1365-2664.13148>.
- Gazoulis, I., et al., 2024. Agroecology and beyond: enhancing ecosystem services provided by natural vegetation and inventing “service weeds”. *Front. Plant Sci.* 15, 1436310. <https://doi.org/10.3389/fpls.2024.1436310>.
- Glaser, M., et al., 2024. Pronounced turnover of vascular plant species in Central European arable fields over 90 years. *Agr. Ecosyst. Environ.* 361, 108798. <https://doi.org/10.1016/j.agee.2023.108798>.
- Griffith, D.M., Veech, J.A., Marsh, C.J., 2016. ‘cooccur: probabilistic species co-occurrence analysis in R’. *Journal of Statistical Software* 69 (Code Snippet 2). <https://doi.org/10.18637/jss.v069.c02>.
- Gallmann, J., et al., 2022. Flower Mapping in Grasslands with Drones and Deep Learning. <https://doi.org/10.22541/au.158740047.73964506>.
- Hartig, F., 2016. DHARMA: Residual Diagnostics for Hierarchical (Multi-Level / Mixed) Regression Models. <https://doi.org/10.32614/CRAN.package.DHARMA>.
- Hernandez-Santin, L., et al., 2019. Identifying species and monitoring understorey from UAS-derived data: a literature review and future directions. *Drones* 3 (1), 9. <https://doi.org/10.3390/drones3010009>.
- Hijmans, R.J., 2010. ‘raster: Geographic Data Analysis and Modeling’. <https://doi.org/10.32614/CRAN.package.raster>.
- Hollander, M., Wolfe, D.A., 1973. *Nonparametric Statistical Methods*. John Wiley & Sons, New York, pp. 115–120.
- Jäger, E.J., et al., 2017. ‘Rothmaler - Exkursionsflora Von Deutschland. Gefäßpflanzen: Atlasband’ (13 ed.) Springer-Spektrum.
- Jocher, G., Chaurasia, A., Qiu, J., 2023. ‘Ultralytics YOLOv8’. <https://github.com/ultralytics/ultralytics>.
- Kaiser, T., Reutter, M., Matzdorf, B., 2019. How to improve the conservation of species-rich grasslands with result-oriented payment schemes? *J. Nat. Conserv.* 52, 125752. <https://doi.org/10.1016/j.jnc.2019.125752>.
- Kassambara, A., 2019. ‘rstatix: Pipe-Friendly Framework for Basic Statistical Tests’. <https://doi.org/10.32614/CRAN.package.rstatix>.
- Kattenborn, T., et al., 2020. Convolutional Neural Networks accurately predict cover fractions of plant species and communities in Unmanned Aerial Vehicle imagery. *Remote Sensing in Ecology and Conservation*. Edited by Horning, N., Clerici, N., 6(4), pp. 472–486. <https://doi.org/10.1002/rse2.146>.

- Keenleyside, C., et al., 2014. 'Results-based Payments for Biodiversity Guidance Handbook: Designing and implementing results-based agri-environment schemes 2014–20'. Prepared for the European Commission, DG Environment, Contract No ENV.B.2/ETU/2013/0046. Institute for European Environmental Policy, London. <https://www.rbpnetwork.eu/media/rbaps-handbook.pdf>.
- Komsta, L., Novomestky, F., 2005. 'moments: Moments, Cumulants, Skewness, Kurtosis and Related Tests'. <https://doi.org/10.32614/CRAN.package.moments>.
- LeCun, Y., Bengio, Y., Hinton, G., 2015. Deep learning. *Nature* 521 (7553), 436–444. <https://doi.org/10.1038/nature14539>.
- Leydesdorff, L., 2005. Similarity measures, author cocitation analysis, and information theory. *J. Am. Soc. Inf. Sci. Technol.* 56 (7), 769–772. <https://doi.org/10.1002/asi.20130>.
- Liu, T., et al., 2018. Comparing fully convolutional networks, random forest, support vector machine, and patch-based deep convolutional neural networks for object-based wetland mapping using images from small unmanned aircraft system. *Giscience & Remote Sensing* 55 (2), 243–264. <https://doi.org/10.1080/15481603.2018.1426091>.
- Lottes, P., et al., 2017. In: UAV-Based Crop and Weed Classification for Smart Farming. IEEE, Singapore, pp. 3024–3031. <https://doi.org/10.1109/ICRA.2017.7989347>.
- Lu, B., He, Y., 2017. Species classification using Unmanned Aerial Vehicle (UAV)-acquired high spatial resolution imagery in a heterogeneous grassland. *ISPRS J. Photogramm. Remote Sens.* 128, 73–85. <https://doi.org/10.1016/j.isprsjprs.2017.03.011>.
- Maitner, B.S., et al., 2018. 'The BIEN R package: a tool to access the botanical information and ecology network (BIEN) database', *Methods in Ecology and Evolution*. Edited by S. McMahon, 9(2), pp. 373–379. <https://doi.org/10.1111/2041-210X.12861>.
- Maitner, B., 2017. 'BIEN: Tools for Accessing the Botanical Information and Ecology Network Database'. <https://doi.org/10.32614/CRAN.package.BIEN>.
- Martins, J.A.C., et al., 2023. Identifying plant species in kettle holes using UAV images and deep learning techniques. *Remote Sens. Ecol. Conserv.* 9 (1), 1–16. <https://doi.org/10.1002/rse2.291>.
- Massfeller, A., et al., 2022. Farmers' acceptance of results-based agri-environmental schemes: a German perspective. *Land Use Policy* 120, 106281. <https://doi.org/10.1016/j.landusepol.2022.106281>.
- Mensah, B., et al., 2024. Advances in weed identification using hyperspectral imaging: a comprehensive review of platform sensors and deep learning techniques. *Journal of Agriculture and Food Research* 18, 101388. <https://doi.org/10.1016/j.jafr.2024.101388>.
- Moss, S.R., et al., 2004. The broadbalk long-term experiment at rothamsted: what has it told us about weeds? *Weed Sci.* 52 (5), 864–873.
- Oppermann, R., et al., 2021. A rapid method for monitoring landscape structure and ecological value in european farmlands: the LISA approach. *Landscape Online* 90, 1–24. <https://doi.org/10.3097/LO.202190>.
- Pavoine, S., 2017. 'adiv: Analysis of Diversity'. <https://doi.org/10.32614/CRAN.package.adiv>.
- Pe'er, G., et al., 2020. Action needed for the EU Common Agricultural Policy to address sustainability challenges', *People and Nature*. Edited by K. Gaston, 2(2), pp. 305–316. <https://doi.org/10.1002/pan3.10080>.
- Pearson, K., 1895. Notes on regression and inheritance in the case of two parents. *Proc. R. Soc. Lond.* 58, 214.
- Piñar Fuentes, J.C., et al., 2021. Impact of grass cover management with herbicides on biodiversity, soil cover and humidity in olive groves in the Southern Iberian. *Agronomy* 11 (3), 412. <https://doi.org/10.3390/agronomy11030412>.
- Preislerová, Z., et al., 2022. Distribution maps of vegetation alliances in Europe. *Appl. Veg. Sci.* 25 (1), e12642.
- R Core Team, 2022. 'R: A Language and Environment for Statistical Computing'. R Foundation for Statistical Computing. <https://www.R-project.org/>.
- Redmon, J., et al., 2016. 'You only look once: unified, real-time object detection', in *2016 IEEE Conference on Computer Vision and Pattern Recognition (CVPR). 2016 IEEE Conference on Computer Vision and Pattern Recognition (CVPR)*, Las Vegas, NV, USA: IEEE, pp. 779–788. <https://doi.org/10.1109/CVPR.2016.91>.
- Roussel, J.R., et al., 2020. lidR: an R package for analysis of Airborne Laser Scanning (ALS) data. *Remote Sens. Environ.* 251, 112061. <https://doi.org/10.1016/j.rse.2020.112061>.
- Schöttker, O., et al., 2023. Monitoring costs of result-based payments for biodiversity conservation: will UAV-assisted remote sensing be the game-changer? *J. Nat. Conserv.* 76, 126494. <https://doi.org/10.1016/j.jnc.2023.126494>.
- Spearman, C., 1904. The proof and measurement of association between two things. *Am. J. Psychol.* 15, 72–101. <https://doi.org/10.2307/1412159>.
- Stache, F., et al., 2023. Adaptive path planning for UAVs for multi-resolution semantic segmentation. *Rob. Auton. Syst.* 159, 104288. <https://doi.org/10.1016/j.robot.2022.104288>.
- Starkey, J., et al., 2012. The impact of agricultural intensification and land-use change on the European arable flora. *Proc. R. Soc. B Biol. Sci.* 279 (1732), 1421–1429. <https://doi.org/10.1098/rspb.2011.1686>.
- Terven, J., Córdoba-Espárza, D.M., Romero-González, J.A., 2023. A comprehensive review of YOLO architectures in computer vision: from YOLOv1 to YOLOv8 and YOLO-NAS. *Mach. Learn. Knowl. Extr.* 5 (4), 1680–1716. <https://doi.org/10.3390/make5040083>.
- Torresani, M., et al., 2024. Grassland vertical height heterogeneity predicts flower and bee diversity: an UAV photogrammetric approach. *Sci. Rep.* 14 (1), 809. <https://doi.org/10.1038/s41598-023-50308-9>.
- Ulber, L., et al., 2009. An on-farm approach to investigate the impact of diversified crop rotations on weed species richness and composition in winter wheat. *Weed Res.* 49 (5), 534–543. <https://doi.org/10.1111/j.1365-3180.2009.00722.x>.
- Veech, J.A., 2013. A probabilistic model for analysing species co-occurrence, *Global Ecology and Biogeography*. Edited by P. Peres-Neto, 22(2), pp. 252–260. <https://doi.org/10.1111/j.1466-8238.2012.00789.x>.
- Wada, K., 2016. 'LabelMe: Image Polygonal Annotation with Python'. <https://github.com/wkentaro/labelme>.
- Wang, K., et al., 2024. Weed detection and recognition in complex wheat fields based on an improved YOLOv7. *Front. Plant Sci.* 15, 1372237. <https://doi.org/10.3389/fpls.2024.1372237>.
- Wang, Z., et al., 2023. 'Revisiting evaluation metrics for semantic segmentation: optimization and evaluation of fine-grained intersection over union'. *arXiv*. <http://arxiv.org/abs/2310.19252>.
- Weigelt, P., König, C., Kreft, H., 2020. GIFT – a Global Inventory of Floras and Traits for macroecology and biogeography. *J. Biogeogr.* 47 (1), 16–43. <https://doi.org/10.1111/jbi.13623>.
- Wolff, F., et al., 2023. RGB vs multispectral imagery: mapping aapa mire plant communities with UAVs. *Ecological Indicators* 148, 110140. <https://doi.org/10.1016/j.ecolind.2023.110140>.
- Wuepper, D., Huber, R., 2022. Comparing effectiveness and return on investment of action- and results-based agri-environmental payments in Switzerland. *Am. J. Agric. Econ.* 104 (5), 1585–1604. <https://doi.org/10.1111/ajae.12284>.
- Yang, X., et al., 2023. Mapping understory plant communities in deciduous forests from Sentinel-2 time series. *Remote Sens. Environ.* 293, 113601. <https://doi.org/10.1016/j.rse.2023.113601>.